communications earth & environment

ARTICLE

https://doi.org/10.1038/s43247-023-00864-9 OPEN

Large obliquity-paced Antarctic ice-volume fluctuations suggest melting by atmospheric and ocean warming during late Oligocene

Swaantje Brzelinski [1✉], André Bornemann [2], Diederik Liebrand [3,4], Tim E. van Peer [3,5], Paul A. Wilson [3] & Oliver Friedrich [1]

The late Oligocene (~27.8–23 My ago) offers an opportunity to study past climate variability under high-CO_2, warmer-than-present and the unipolar (Antarctic) glaciated state. Here, we present new high-resolution geochemical records from exquisitely well-preserved benthic foraminifera for the late Oligocene, an interval for which Antarctic ice-sheet size and stability are debated. Our records indicate four obliquity-paced glacial-interglacial cycles with ice-volume changes of up to ~70% of the modern Antarctic ice-sheet. The amplitude of ice-volume change during these late Oligocene glacial-interglacial cycles is comparable to that of the late Pliocene and early Pleistocene. Ice-volume estimates for interglacials are small enough to be accommodated by a land-based Antarctic ice-sheet but, for three of the four glacials studied, our calculations imply that ice sheets likely advanced beyond the Antarctic coastline onto the shelves. Our findings suggest an Antarctic ice-sheet vulnerable to melting driven by both bottom-up (ocean) and top-down (atmospheric) warming under late Oligocene warmer-than-present climate conditions.

[1] Institute of Earth Sciences, Heidelberg University, Heidelberg, Germany. [2] Bundesanstalt für Geowissenschaften und Rohstoffe, Hannover, Germany. [3] National Oceanography Centre Southampton, University of Southampton, Waterfront Campus, Southampton, UK. [4] Present address: Department of Earth and Environmental Sciences, The University of Manchester, Manchester, UK. [5] Present address: School of Geography Geology and Environment, University of Leicester, Leicester, UK. ✉email: swaantje.brzelinski@gmail.com

Earth's climate during the Oligocene epoch (~34 to 23 Ma) was poised in a unipolar (Antarctic) glacial state[1], between the much warmer climate state[2] of the early Cenozoic era, in which the continents were mostly ice-free, and the much colder climate state of the late Cenozoic[2], when major ice sheets also waxed and waned in the Northern Hemisphere[3]. The Oligocene climate history began with the establishment of large sustained ice sheets on Antarctica at the Eocene–Oligocene Transition (~33.6 Ma ago)[4,5], followed by the colder but highly variable Mid-Oligocene Glacial Interval (~28–26.3 Ma)[6]. A warming climate characterised the late Oligocene warming phase (LOW) between ~26.3 and 23.7 Ma[6] that was abruptly terminated by a major transient glaciation at the Oligocene-Miocene Transition (OMT; ~23.7–22.7 Ma ago; Fig. 1a)[4,7]. Thus, the long-term evolution of the Antarctic ice-sheet (AIS) across the Oligocene is now relatively well established[4]. Yet the astronomical pacemaker of the early Cenozoic AIS is debated. Ice-proximal sedimentological records are interpreted to indicate significant, recurring obliquity-paced AIS oscillations[8–11] but stratigraphic age control in such archives is often challenging. Even in ice-distal pelagic marine sequences, where age control is typically stronger, the astronomical imprint on benthic foraminiferal oxygen isotope ($\delta^{18}O_{BF}$) records is enigmatic with pronounced spatial and temporal variability in both the ~400- and 100-kyr eccentricity and 40-kyr obliquity cycles[6,12–15]. A further complicating observation is that $\delta^{18}O_{BF}$-based ice-volume reconstructions for the AIS yield sharply conflicting conclusions over the size and stability of the AIS during the LOW interval. Using a $\delta^{18}O_{BF}$ record from Site 1264 (South Atlantic Ocean, Fig. 2a), ref. [6] inferred episodes of high-amplitude variability in $\delta^{18}O_{BF}$ requiring waxing and waning by at least ~85 to 110% of the present-day volume of the East Antarctic Ice Sheet (EAIS) on ~100-kyr timescales with a distinct overall ice-volume decrease from about 27 to 24 Ma (Fig. 2a). In contrast, a heavily glaciated Antarctic continent from 27.8 to 24.5 Ma with ice sheets approaching or exceeding their modern-size and no indications of significant ice-sheet disintegration is invoked based on a $\delta^{18}O_{BF}$ record from Maud Rise (Antarctica; Fig. 2a)[16]. One major source of uncertainty contributing to these conflicting interpretations of the Antarctic glaciation history during the late Oligocene[6,16] is the undocumented contribution to these $\delta^{18}O_{BF}$ records of bottom-water temperature (BWT) versus ice-volume change[4], highlighting the need for high-quality independent records of BWT to isolate the ice-volume signal from $\delta^{18}O_{BF}$.

Here, we reconstruct changes in seawater $\delta^{18}O$ ($\delta^{18}O_{sw}$)—a proxy for continental ice-volume[4]—by determining Mg/Ca-derived BWT on the same samples as $\delta^{18}O_{BF}$. Our approach (Methods and Supplementary Information) follows established protocols[4,17]. Our $\delta^{18}O_{sw}$ record comes from Integrated Ocean Drilling Programme (IODP) Site U1406 situated in the north-western Atlantic Ocean (~40 °N and 3814 m depth)[18]. Oligocene strata from Site U1406 comprise rapidly deposited (up to 3 cm/kyr in our study interval)[19] sediment drift deposits. Our records are based on exquisitely well-preserved foraminifera (Supplementary Note 1) ($\delta^{18}O_{BF}$: *Cibicidoides mundulus* and *Oridorsalis umbonatus;* Supplementary Fig. 1; Mg/Ca: *O. umbonatus*; Supplementary Fig. 2) and they are of high temporal resolution (600–1000 years) with an independent, astronomically-tuned age model[19]. Our focus, the late Oligocene, is an interval suggested to be strongly influenced by 400- and 100-kyr eccentricity cycles in $\delta^{18}O_{BF}$[6,12] and low obliquity sensitivity (S_{obl})[20] (Fig. 1b, c). The fidelity of our coupled $\delta^{18}O_{BF}$-Mg/Ca measurements is high because (i) our records are unaffected by post-depositional diagenetic alteration (Supplementary Fig. 2) and sampling effects (Methods) and (ii) we used robust calibrations to calculate BWT and $\delta^{18}O_{sw}$ from our $\delta^{18}O_{BF}$ and Mg/Ca data (Methods and Supplementary Notes 3 and 4). Our calculations were made taking care to consider temporal variability in seawater chemistry, i.e., Mg/Ca_{sw}, *pH*, and the past oxygen-isotope composition of the AIS ($\delta^{18}O_{ice}$). Our $\delta^{18}O_{sw}$ reconstruction yields an average uncertainty of ±0.25‰ (Fig. 2d) based on calculated 95% probability intervals through Monte Carlo Simulations (Methods). Based on these analyses, we document substantial obliquity-paced ice-volume changes in Antarctica between ~25.94 and 25.78 Ma.

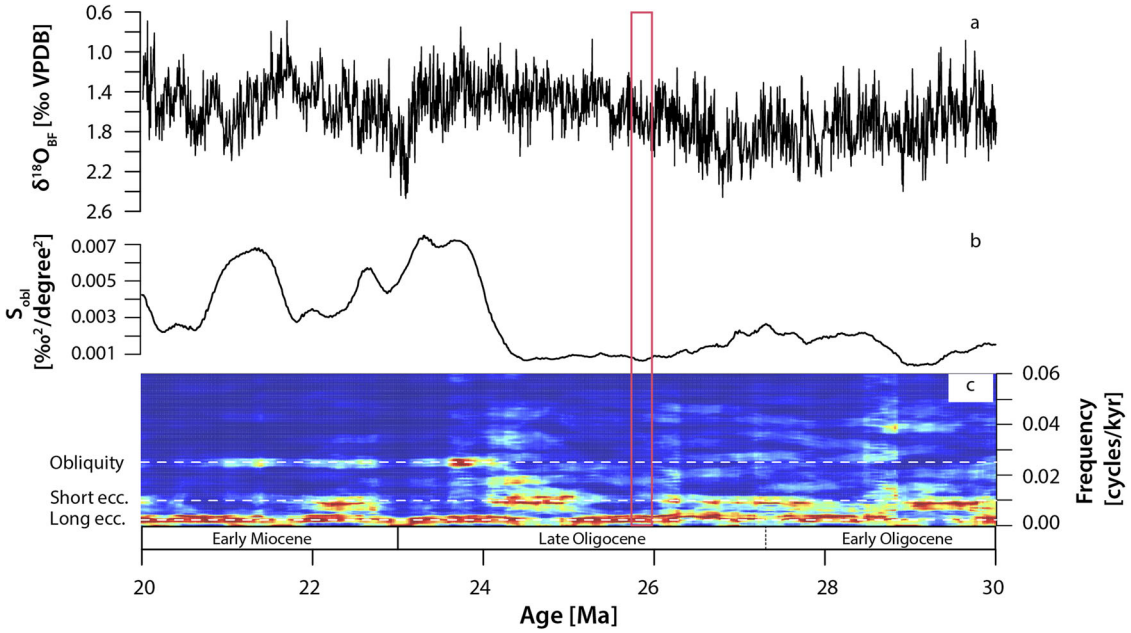

Fig. 1 Early Oligocene to Early Miocene oxygen-isotope data and orbital variability. a Oxygen isotope ($\delta^{18}O_{BF}$) megasplice compilation[40] spanning ~30–20 Ma. **b** Obliquity sensitivity (S_{obl}) determined as the ratio between the variance in the $\delta^{18}O_{BF}$ megasplice record and the La2004 obliquity solution[21] (calculated following ref. [20]). **c** Evolutive power spectra of $\delta^{18}O_{BF}$ megasplice compilation shown in (a) calculated following R-script of ref. [20] (red colours indicate maximum power, blue colours indicate minimum power). Red box indicates the study interval presented herein spanning ~25.94–25.78 Ma.

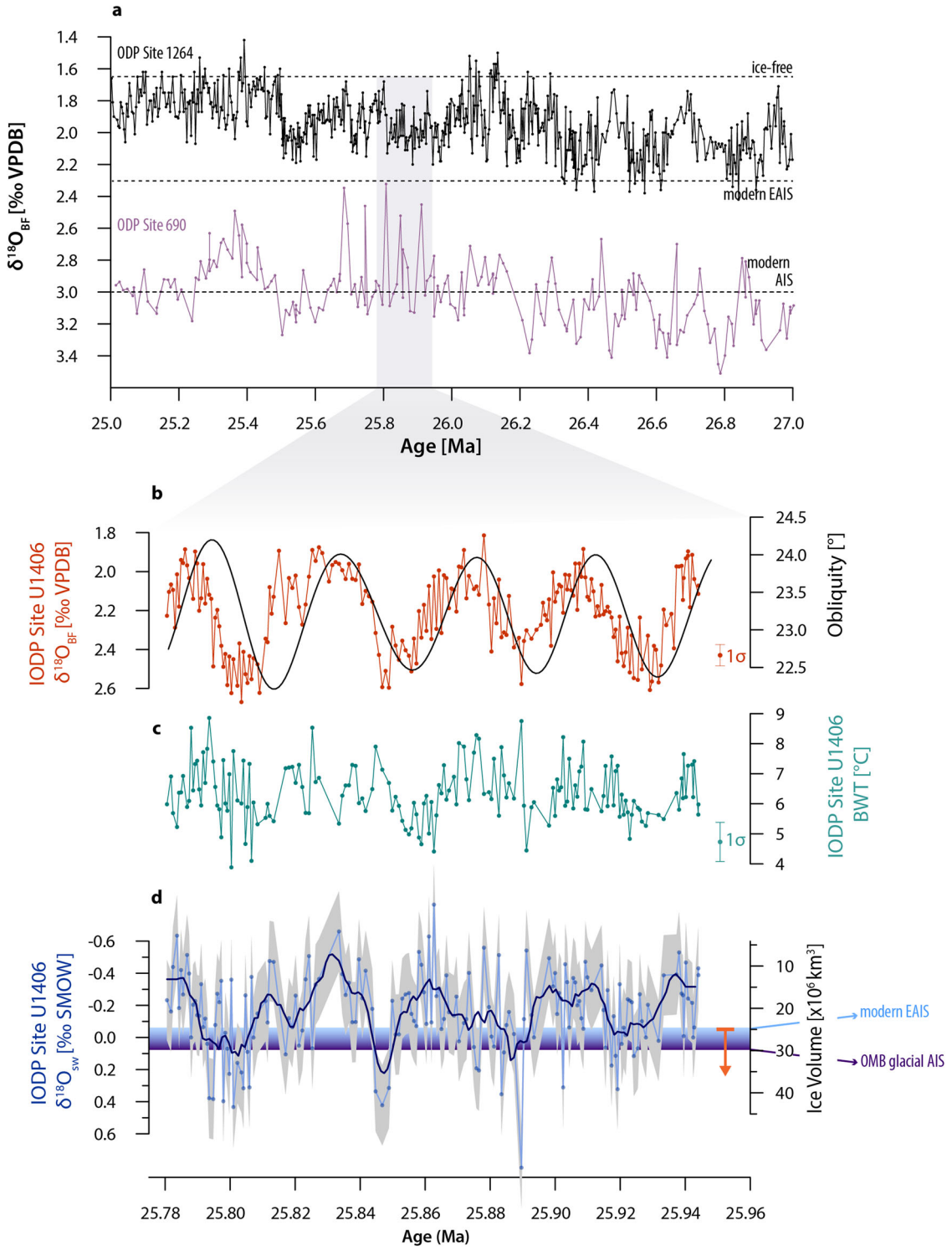

Fig. 2 Antarctic climate evolution during the late Oligocene. a Late Oligocene (27–25 Ma) $\delta^{18}O_{BF}$ records (*C. mundulus*; in ‰ VPDB) of ODP Site 1264[6] (black) and Site 690[16] (violet). Dashed lines indicate ice-free scenario and present-day-sized EAIS[26] for Site 1264[6] and present-day sized AIS[26] for Site 690[16]. **b** IODP Site U1406 $\delta^{18}O_{BF}$ record (in ‰ VPDB; *C. mundulus* has been normalised to *O. umbonatus*, Supplementary Note 2) (red) together with the orbital solution for obliquity (black)[21]. **c** IODP Site U1406 Mg/Ca-based BWT estimates (in °C; green). **d** IODP Site U1406 $\delta^{18}O_{sw}$ record (in ‰ SMOW; blue) with 5-pt smoother (dark blue line) and ±0.25 ‰ uncertainty resulting from Monte Carlo Simulations (grey envelop; Methods and Supplementary Information). Red bar and arrow indicate ice-volumes bigger than the modern continental ice-volume (i.e., EAIS) and, hence, the existence of marine-based ice-sheets. Vertical bars in (**b**) and (**c**) indicate the 1σ standard deviation associated with the individual Site U1406 proxy records. Study interval (~25.94–25.78 Ma) indicated by violet shading in (**a**). Shaded area in (**d**) represents the range between the size of the modern EAIS (~24.6×10^6 km^3)[26] and the modelled glacial ice-volume at the Oligocene-Miocene boundary (OMB, ~23 Ma ago)[35].

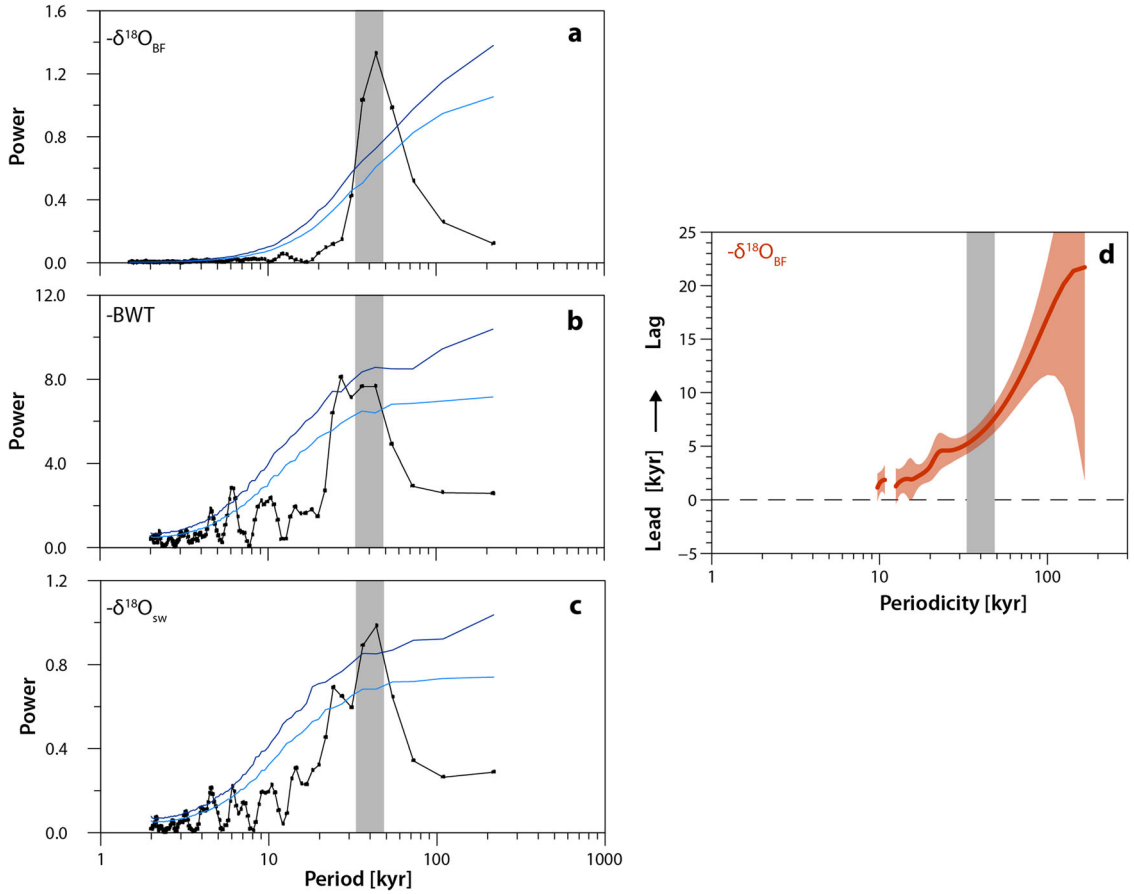

Fig. 3 Spectral analysis of the U1406 $\delta^{18}O_{BF}$, BWT and $\delta^{18}O_{sw}$ records. REDFIT spectral analysis[66] of our $\delta^{18}O_{BF}$ (**a**), BWT (**b**) and $\delta^{18}O_{sw}$ (**c**) records. Monte Carlo confidence intervals of 80% (light blue) and 90% (dark blue). **d** Blackman–Tukey cross-spectral phase estimate between the $\delta^{18}O_{BF}$ time series (at 95% significance) and the orbital solution for obliquity[21] (converted to lag times in kyr). The signal at the obliquity frequency is highlighted with grey bars.

Results and discussion

Glacial-interglacial variability during the late Oligocene. Our $\delta^{18}O_{BF}$ record shows four well-pronounced sinusoidally shaped oscillations (hereafter, glacial-interglacial cycles) in $\delta^{18}O_{BF}$ between 1.8‰ and 2.7‰ (Fig. 2b). Spectral analysis of the record (Fig. 3) reveals a strong 40-kyr signal related to obliquity. Comparison to the astronomical solution for obliquity[21] shows correspondence of high (low) $\delta^{18}O_{BF}$ values with low (high) obliquity (Fig. 2b), with a phase lag of 6.2 kyr (Fig. 3). This phase lag is similar to those reported (~6.5–8 kyr) between $\delta^{18}O_{BF}$ and Earth's obliquity for the Pleistocene and late Pliocene[22]. Calculated BWTs also show obliquity-paced fluctuations (Figs. 2c and 3) and vary by 2 to 3 °C over the study interval. Cooler BWTs (~4.5–6 °C) correspond to intervals of high $\delta^{18}O_{BF}$ while intervals of warmer BWTs (~6–8 °C; Fig. 2c) occur when $\delta^{18}O_{BF}$ is lower.

Amplitude of $\delta^{18}O_{sw}$ fluctuations. Next, we use our Mg/Ca-based BWTs together with the $\delta^{18}O_{BF}$ time series to deconvolve the $\delta^{18}O_{sw}$ component of $\delta^{18}O_{BF}$. The resulting $\delta^{18}O_{sw}$ record mimics the glacial-interglacial cyclicity of our $\delta^{18}O_{BF}$ record (Fig. 2b, d) and indicates obliquity-paced waxing and waning of late Oligocene land ice (in Antarctica). Glacials are characterised by higher $\delta^{18}O_{sw}$ (0 to 0.20‰) than interglacials (−0.25 to −0.55‰). The amplitude of glacial-interglacial change revealed by our $\delta^{18}O_{sw}$ record ranges from ~0.4 to ~0.6‰ (average of ~0.5‰) and is comparable to those determined for the late Oligocene in a less well resolved Mg/Ca record from the equatorial Pacific (0.4 to 0.6‰; ODP Site 1218)[23]. We estimated ice-volume from our $\delta^{18}O_{sw}$ record by assuming the mean isotopic composition of land ice ($\delta^{18}O_{ice}$) was −42‰[24,25] (Supplementary Fig. 4; Supplementary Notes 5 and 6) and inferring a modern AIS baseline for $\delta^{18}O_{sw}$ of 0‰ (SMOW), equivalent to ~26.9 million km^3 ($\times 10^6$ km^3) of ice[26] with a growth of 3.8×10^6 km^3 of ice per 0.1‰ change in $\delta^{18}O_{sw}$[6,27] (Supplementary Fig. 4). This approach yields interglacial ice-volume estimates of ~6–17 ± 9.5×10^6 km^3 of ice (~22–65 % of the modern AIS) and glacial ice-volume estimates of ~27–34.5 ± 9.5×10^6 km^3 of ice (~100–128 % of the modern AIS) and, on average, results in glacial-interglacial waxing and waning of ~19 ± 9.5×10^6 km^3 of ice, equivalent to ice gain/loss of ~70%. Our higher-than-modern Antarctic ice-volume estimates for late Oligocene glacials cannot be explained by ice-sheet build-up in the Northern Hemisphere. While the sporadic presence of potential ice-rafted debris in the Greenland Sea and the Arctic Ocean[28–30] has been used to infer the presence of Northern Hemisphere ice-sheets as early as the Eocene, modelling[25] and proxy-based[1,31] studies rule out the suggestion of extensive ice sheets in the Northern Hemisphere this early in the Cenozoic while leaving open the possibility that short-lived, isolated and small mountain glaciers existed there throughout most of the Cenozoic[32,33]. An Antarctic palaeotopographic reconstruction for the Oligocene-Miocene boundary (OMB, ca. 23 Ma) that incorporates physical processes including erosion, tectonics and isostatic feedback suggests a ~15% larger land area above sea-level than at the present-day[34]. Based on this OMB palaeotopography[34], ice-sheet modelling experiments for the

OMB[35] suggest that Antarctica was able to support a glacial ice-sheet ~110% of its present volume (29.65×10^6 km^3)[35] with ice-sheet margins extending into the ocean. While some studies on the eastern Wilkes Land margin[9,36,37] suggest temperate conditions during the late Oligocene, those data are of very low temporal resolution and therefore cannot be used to assess astronomically paced change. On the other hand, our estimates of AIS volume maxima for the late Oligocene glacials (~27–$34.5 \pm 9.5 \times 10^6$ km^3) resonate well with the latest AIS model reconstructions showing larger than modern ice volumes for a cold climate OMB state[35]. Support for our interpretations is also provided by the presence of ice-rafted clasts in late Oligocene sections of the Polonez Cove Formation (King George Island, Antarctic Peninsula)[38] suggesting that marine-based ice drained into the Weddell Sea and by evidence that marine-terminating glaciers extended periodically beyond the coast in the Ross Sea Embayment[39] during our study interval.

Waxing and waning of the late Oligocene AIS. With fluctuations on the order of ~$19 \pm 9.5 \times 10^6$ km^3 over individual obliquity cycles, our data suggest that the AIS was highly responsive to obliquity-dominated insolation forcing during this particular Oligocene time interval. Other records spanning our study interval imply a different picture. Ice-volume estimates from one record on Maud Rise[16] imply a heavily glaciated Antarctic continent with only modest variability between intervals with an AIS slightly smaller than the present day to intervals with an AIS slightly larger than the present day ($\delta^{18}O_{BF}$ values between 2.3 and 3.1‰)[26] (Fig. 2a). Another record of ice-volume estimates for our study interval[6] suggests ice-volume fluctuations ranging between an almost ice-free state and an ice-volume smaller than the modern EAIS ($\Delta_{ice\text{-}volume}$ of $15–20 \times 10^6$ km^3)[26] (Fig. 2a). Our record, however, shows a glacial-interglacial structure with high amplitude change from the lower ice-volume estimates of ref. [6] (mainly during interglacials) to the higher ice-volume estimates of ref. [16] during glacials (Fig. 2a, d).

Ref. [20] determined $\delta^{18}O_{BF}$ obliquity sensitivity (S_{obl}) by dividing the obliquity variance in a $\delta^{18}O_{BF}$ 'megasplice' record[40] by the variance of the numerical obliquity solution[21] to detect a terrestrial versus marine-based AIS during the Oligo–Miocene. Because the marine-based portion of the AIS is considered susceptible to upwelling of warm deep water from the circum-Antarctic Southern Ocean onto the continental margin on obliquity timescales[9,41], a marked increase in S_{obl} around 24.5 My ago was interpreted to indicate that the initiation of Antarctic ice sheets large enough to have been influenced in this way[20]. Orbitally-paced expansion of marine-based ice sheets from the OMT onwards is also suggested by a recent sea-surface temperature compilation from the Ross Sea[42]. Our new obliquity-paced $\delta^{18}O_{sw}$ record from Site U1406 reveals that major obliquity-paced Antarctic glacial-interglacial cycles occurred at least 1.5 My before the OMT.

Our estimates of interglacial ice-volume are markedly smaller than the present day EAIS[26], strongly suggesting that these late Oligocene interglacial AISs were wholly land-based. However, while there are uncertainties associated with both our calculations and the land-ice capacity of Antarctica[34,35], our ice-volume estimates suggest that, for three of the four glacials studied, the late Oligocene AIS was not only larger than the present day AIS[26] but also in the same range as those modelled for the OMB which included floating ice shelves[35] (Fig. 2d). This observation suggests that, during the obliquity-paced glacials that we document, the AIS advanced beyond the Antarctic coastline into marine environments introducing ocean-induced melting as a mechanism of obliquity-paced deglaciation earlier than previously proposed[20,42]. Our records show deglaciations resulting in reductions in size of the late Oligocene AIS to ~50% of its precursor maximum glacial volume, indicating vulnerability to both bottom-up (ocean) and top-down (atmospheric) warming (Fig. 2d).

Obliquity forcing of the late Oligocene AIS. The $\delta^{18}O_{sw}$ record from Site U1406 provides clear evidence of a highly dynamic cryosphere during the late Oligocene epoch between ~25.94 and 25.78 Ma and shows distinct cyclicity in the obliquity band (Fig. 3). We infer that high amplitude obliquity cycles[21] drive the observed glacial-interglacial cyclicity of our $\delta^{18}O_{sw}$ data via predominantly obliquity-paced variability in deep-water circulation patterns across the Antarctic continental margin[9,20]. During obliquity maxima, westerly winds and the polar front are shifted polewards. Under these conditions, the associated Ekman transport (under influence of the Westerlies) promotes enhanced upwelling and advection of warm deep water from the circum-Antarctic Southern Ocean into grounding zones and ice-shelf cavities, causing ice melt and ice sheet retreat[43,44]. During glacials, when the angle of Earth's tilt was decreased, westerly winds and surface oceanic fronts were positioned more equatorward, generating a more stratified ocean with reduced upwelling of warm water across the Antarctic shelf allowing ice sheets to grow and expand across the shelf[9,20].

The strong imprint of obliquity on our records contradicts the suggestion of persistently low S_{obl} prior to 24.5 Ma that was reconstructed for our study interval using a composite $\delta^{18}O_{BF}$ record[20] (Fig. 1b). Our results provide robust evidence to support the obliquity-paced glacial-interglacial facies changes that have been inferred in sediments of late Oligocene age (25.99 to 25.25 Ma) from off-shore the Wilkes Land margin (East Antarctica, IODP Site U1356)[9]. This is an important result because, while we can be confident that the Wilkes Land margin record reflects environmental changes influencing the size of the EAIS, our records quantify the overall size of the AIS involved and benefit from strong age control so we can now be sure of the astronomical pacemaker responsible.

Obliquity-paced $\delta^{18}O_{sw}$ fluctuations during unipolar and bipolar glaciated climate states. Our high-resolution $\delta^{18}O_{sw}$ record yields novel insight into the ice ages of the understudied early Cenozoic unipolar icehouse state. Obliquity-paced glacial-interglacial $\delta^{18}O_{sw}$ changes reported from the late Pliocene (~3.6–2.5 Ma; 0.34 to 0.55‰) as well as the early Pleistocene (~2.5–1.8 Ma; 0.4 to 0.6‰)[45,46] show similar amplitude changes to those displayed in our late Oligocene record (average of ~0.5‰; Fig. 4). In contrast to the unipolar icehouse state of the late Oligocene, however, those Plio-Pleistocene changes were driven by the advance and retreat of ice-sheets in both the Southern[17] and especially the Northern Hemisphere[45,46]. The two most important factors controlling global ice-volume on astronomical timescales are insolation and atmospheric CO_2 concentrations[25,47]. Existing CO_2 reconstructions for the late Oligocene (between 28.78 and 23.48 Ma) are sparse but display CO_2 variations between ~410 and 730 ppmv[48]. These CO_2 concentrations are significantly higher than those reported for the late Pliocene (450–250 ppmv) and early Pleistocene (360–250 ppmv)[48,49], yet glacial-interglacial $\delta^{18}O_{sw}$ changes are similar (Fig. 4). Our new data and observations further demonstrate that the AIS was highly susceptible to melting driven by both bottom-up (ocean) and top-down (atmospheric) warming under warmer-than-present, high-CO_2 conditions of the late Oligocene.

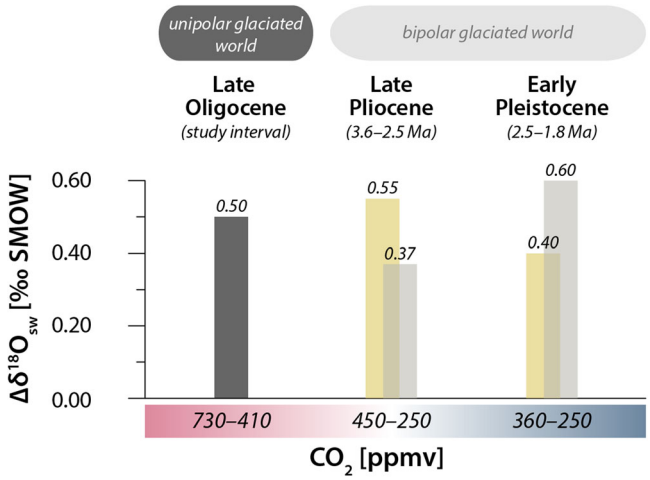

Fig. 4 Obliquity-paced $\delta^{18}O_{sw}$ fluctuations during unipolar and bipolar glaciated climate states. Comparison of amplitude changes in $\delta^{18}O_{sw}$ ($\Delta\delta^{18}O_{sw}$) during the unipolar-glaciated late Oligocene (25.94–25.78 Ma; this study; dark grey), the late Pliocene (3.6–2.5 Ma) and the early Pleistocene (2.5–1.8 Ma) (yellow: ref. [45]; light grey: ref. [46]) under different radiative forcing conditions (atmospheric CO_2 concentrations)[48,49]. Late Oligocene CO_2 range from 28.78 to 23.48 Ma[48].

Materials and methods

Sample material and processing. Sediments retrieved from IODP Site U1406 (J-Anomaly Ridge, northwestern Atlantic Ocean[19]) yielded a largely complete upper Oligocene (Chattian) sequence as indicated by shipboard sedimentological, biostratigraphical (planktic foraminifera, calcareous nannoplankton, radiolaria), and magnetostratigraphical data[19] and subsequent shore-based investigations using XRF core scanning[48], magnetostratigraphy[49], and dinoflagellate-cyst biostratigraphy[50]. The sampled core material consists of clay-rich drift sediments, characterised by brown to green nannofossil ooze[19] and sedimentation rates of up to 3 cm/kyr[19,49]. Samples with a volume of ~20 cm^3 were collected from 141.29 to 145.90 m revised CCSF-A (core composite depth below seafloor, method 'A'), following the revised splice published by ref. [48]. Sample ages were calculated using the astronomically tuned timescale of ref. [20], which was created by orbitally tuning the Site U1406 high-resolution XRF-based $CaCO_3$ record to the astronomical solution for obliquity of ref. [22]. We sampled at a spacing of 2–4 cm to generate a high-resolution, sub-orbital benthic foraminiferal oxygen isotope ($\delta^{18}O_{BF}$) and Mg/Ca data set for the Late Oligocene between 25.78 and 25.94 Ma. After drying in an oven at 40 °C, samples were wet-sieved over a 63 µm sieve with deionized water. Subsequently, between 2 and 15 individuals of the benthic foraminiferal taxa *Oridorsalis umbonatus* or *Cibicidoides mundulus* were picked from the >125 µm fraction, weighted and isolated for geochemical analyses.

Foraminiferal preservation. The preservation of benthic foraminifera was determined via reflected light microscope and scanning electron microscope (SEM) imaging (Supplementary Fig. 2). The resulting images show that Late Oligocene tests from Site U1406 are of exceptional, glassy[50] preservation (Supplementary Fig. 2) that allows the acquisition of high-quality geochemical data. In addition, information on potential susceptibility to dissolution of the sample material was obtained by studying the shell fragmentation index (FI, Supplementary Fig. 7). Results were plotted against $CaCO_3$ (wt%) of the samples studied and indicate no correlation. Furthermore, U1406 FI values ≤10% (Supplementary Fig. 7) are significantly lower than those presented for studies from the Eocene[51] and Pliocene[52]. We thus conclude that dissolution did not influence the benthic foraminiferal species used for geochemical analysis in this study.

Stable isotopes. Stable oxygen isotopes ($\delta^{18}O_{BF}$) for Site U1406 were primarily derived from the benthic foraminiferal taxa *Oridorsalis umbonatus* and, where not abundant, substituted by analyses on *Cibicidoides mundulus*. Constant and predictable offsets from seawater equilibrium values make both species reliable and frequently used deep-sea stable isotope tracers[53–55]. For stable isotope analyses, ~20–80 µg of the sample material has been analysed using a ThermoFinnigan MAT253Plus gas source mass spectrometer equipped with a Thermo Fisher Scientific Kiel IV carbonate device at Heidelberg University. Values are reported relative to the Vienna Pee Dee Belemnite through the analysis of an in-house standard (Solnhofen limestone) calibrated to IAEA-603. The precision of the $\delta^{18}O_{BF}$ analyses is better than 0.06‰. Measured $\delta^{18}O_{BF}$ values of *C. mundulus* were adjusted to *O. umbonatus* values by adding 0.37‰ after calculating the average interspecies offset between *C. mundulus* and *O. umbonatus* (Supplementary Fig. 1). This isotopic correction factor applied to *C. mundulus* values is in close agreement with recent studies (0.4‰[14], 0.34‰[53]) that infer rather similar offsets (Supplementary Note 2).

Trace-metal analysis and Mg/Ca-based bottom-water palaeothermometry. We performed trace-metal analysis (Mg/Ca, Mn/Ca, Fe/Ca) on specimens of the shallow infaunal dwelling benthic foraminifer *O. umbonatus* only (Supplementary Information). For Mg/Ca analysis, ~150–200 µg of test fragments were cleaned following the protocol of ref. [56]. Following crushing, subsamples were cleaned for the removal of clays with Milli-Q ultrapure water (18.2 Ω) and methanol (CH_4O, ROTISOLV ≥99.98%). Remaining organic material was removed by oxidative cleaning using 250 µl of an oxidising agent (120 µl of 30% H_2O_2 added to 12 ml of 0.1 M NaOH). Reductive cleaning that involves bathing the sample in a hot buffered solution of hydrazine was omitted because it has been shown to lower the Mg/Ca ratio by partial dissolution of foraminiferal calcite (see ref. [56,57] for detailed discussion). Thereafter, samples were visually inspected under a binocular microscope to remove large non-carbonate particles with a fine brush. Subsequently, a weak acid leach was applied to remove any re-adsorbed contaminants from the surface of the foraminifer tests by adding 250 µl of 0.001 M HNO_3 after which samples were dissolved in trace metal pure 0.075 M HNO_3 to a final volume of 500 µl. Samples were analysed using an Agilent Inductively Coupled Plasma-Optical Emission Spectrometer 720 at Heidelberg University. Reported Mg/Ca values were normalised relative to the ECRM 752-1 standard with a reference value of 3.762 mmol/mol[58]. To ensure instrumental precision, an internal consistency standard was monitored every 12 samples with a precision of ±0.03% (1σ). To assess the potential influence of contamination with clay, Fe-oxide or Mn-oxide coatings not removed during the Mg/Ca cleaning process, we also monitored Al, Fe and Mn contents during Mg/Ca analysis (Supplementary Note 3 and Supplementary Fig. 4).

BWTs based on Mg/Ca ratios of *O. umbonatus* were calculated using the species-specific, exponential calibration for *O. umbonatus* of ref. [59] because the range of Mg/Ca ratios observed at Site U1406 (1.09–1.92 mmol/mol) is only captured within the calibration range of this specific calibration (1.09–3.43 mmol/mol) than compared to other available calibrations (for a review see Table 2 of ref. [60]). Furthermore, the chosen calibration covers a BWT range of 0.8 to 9.9 °C more appropriate than other calibrations[60] for the late Oligocene interval which was overall warmer than the present day.

$$Mg/Ca_c^{t=t} = \frac{Mg/Ca_{sw}^{t=t}}{Mg/Ca_{sw}^{t=0}} \times B\exp^{A\times BWT} \quad (1)$$

where Mg/Ca_c is the Mg/Ca of the foraminiferal calcite, $Mg/Ca_{sw}^{t=t}$ is seawater Mg/Ca estimated for the Late Oligocene (3.6 mol/mol)[61], and $Mg/Ca_{sw}^{t=0}$ is seawater Mg/Ca of the modern ocean (5.2 mol/mol)[62], BWT is the bottom-water temperature in degrees Celsius, and A (0.114 ± 0.02) and B (1.008 ± 0.08) are species-specific constants for *O. umbonatus*[59,63]. Because this calibration is based on oxidative and reductive cleaning of foraminiferal tests, whereas only oxidative cleaning has been applied on foraminiferal tests in this thesis, measured Mg/Ca values were adjusted by reducing each value by 10%[56].

Late Oligocene $\delta^{18}O_{sw}$ reconstruction. Coupled Mg/Ca-oxygen isotope measurements enable the $\delta^{18}O$ paleotemperature equation to be solved for past $\delta^{18}O_{sw}$ (relative to the Standard Mean Ocean Water [SMOW]) by using the equation of ref. [64]:

$$\delta^{18}O_{sw} = \frac{BWT - 16.9}{4.0} + \delta^{18}O_{BF} \quad (2)$$

where T is the Mg/Ca-based BWT estimate, $\delta^{18}O_{BF}$ is the measured benthic foraminiferal oxygen isotope value, and $\delta^{18}O_{sw}$ is past seawater $\delta^{18}O$. We added 0.27‰ to our data to convert all values to SMOW. The uncertainty associated with our $\delta^{18}O_{sw}$ reconstruction from Site U1406 was determined through a Monte Carlo Simulation yielding 1σ probability intervals. The Monte Carlo Simulation relies on the assumption that the uncertainty in our $\delta^{18}O_{sw}$ record derives from errors associated with the $\delta^{18}O_{sw}$ reconstruction[65] itself, the analytical precision of $\delta^{18}O_{BF}$ measurements (±0.06‰) and uncertainties in BWT estimates. The uncertainty in BWT estimates is based on the analytical precision of Mg/Ca measurements (±0.03 mmol/mol) and the error associated with the BWT calibration constants[63]. Individual data points were randomly sampled 14,000 times within their proxy uncertainties. The mean propagated uncertainty of the $\delta^{18}O_{sw}$ estimate is ±0.25‰.

Spectral analysis. We applied the REDFIT spectral analysis[66] using the Paleontological Statistics Software Package (PAST)[67]. Before analysis, our $\delta^{18}O_{BF}$, BWT, and $\delta^{18}O_{sw}$ records were linearly detrended. The $\delta^{18}O_{BF}$ time series was interpolated at 0.75 kyr, and BWT and $\delta^{18}O_{sw}$ were interpolated at 1 kyr. All three data sets (Fig. 3) show a distinct peak at the obliquity frequency. We applied Blackman–Tukey cross-spectral phase estimate between the $\delta^{18}O_{BF}$ and the orbital solution for obliquity[21] using the AnalySeries software package version 2.0.8[68]. Results were converted to lag times in kyr. Compared with the frequency modulation of obliquity, there is a relative lag of 6.2 kyr for $\delta^{18}O_{BF}$ (Fig. 3).

Data availability

Underlying data for the main manuscript figures are available via https://doi.org/10.1594/PANGAEA.938936.

Received: 6 December 2022; Accepted: 24 May 2023;
Published online: 22 June 2023

References

1. Spray, J. F. et al. North Atlantic evidence for a unipolar icehouse climate state at the Eocene-Oligocene Transition. *Paleoceanogr. Paleoclimatol.* **34**, 1124–1138 (2019).
2. Westerhold, T. et al. An astronomically dated record of Earth's climate and its predictability over the last 66 million years. *Science.* **369**, 1383–1388 (2020).
3. Bailey, I. et al. An alternative suggestion for the Pliocene onset of major northern hemisphere glaciation based on the geochemical provenance of North Atlantic Ocean ice-rafted debris. *Quat. Sci. Rev.* **75**, 181–194 (2013).
4. Lear, C. H., Elderfield, H. & Wilson, P. A. Cenozoic deep-sea temperatures and global ice volumes from Mg/Ca in benthic foraminiferal calcite. *Science.* **287**, 269–272 (2000).
5. Coxall, H. K., Wilson, P. A., Pälike, H., Lear, C. H. & Backman, J. Rapid stepwise onset of Antarctic glaciation and deeper calcite compensation in the Pacific Ocean. *Nature* **433**, 53–57 (2005).
6. Liebrand, D. et al. Evolution of the early Antarctic ice ages. *Proc. Natl. Acad. Sci. USA* **114**, 3867–3872 (2017).
7. Zachos, J. C., Flower, B. P. & Paul, H. Orbitally paced climate oscillations across the Oligocene/Miocene boundary. *Nature* **388**, 567–570 (1997).
8. Naish, T. R. et al. Orbitally induced oscillations in the East Antarctic ice sheet at the Oligocene/Miocene boundary. *Nature* **413**, 719–723 (2001).
9. Salabarnada, A. et al. Paleoceanography and ice sheet variability offshore Wilkes Land, Antarctica—Part 1: insights from late Oligocene astronomically paced contourite sedimentation. *Clim. Past* **14**, 991–1014 (2018).
10. Galeotti, S. et al. Antarctic Ice Sheet variability across the Eocene-Oligocene boundary climate transition. *Science.* **352**, 76–80 (2016).
11. Dunbar, G. B., Naish, T. R., Barrett, P. J., Fielding, C. R. & Powell, R. D. Constraining the amplitude of late oligocene bathymetric changes in western Ross Sea during orbitally-induced oscillations in the East Antarctic Ice Sheet: (1) implications for glacimarine sequence stratigraphic models. *Palaeogeogr. Palaeoclimatol. Palaeoecol.* **260**, 50–65 (2008).
12. Pälike, H. et al. The heartbeat of the Oligocene climate system. *Science.* **314**, 1894–1898 (2006).
13. Pälike, H., Frazier, J. & Zachos, J. C. Extended orbitally forced palaeoclimatic records from the equatorial Atlantic Ceara Rise. *Quat. Sci. Rev.* **25**, 3138–3149 (2006).
14. Billups, K., Pälike, H., Channell, J. E. T., Zachos, J. C. & Shackleton, N. J. Astronomic calibration of the late oligocene through early Miocene geomagnetic polarity time scale. *Earth Planet. Sci. Lett.* **224**, 33–44 (2004).
15. Zachos, J. C., Shackleton, N. J., Revenaugh, J. S., Pälike, H. & Flower, B. P. Climate response to orbital forcing across the oligocene-miocene boundary. *Science.* **292**, 274–278 (2001).
16. Hauptvogel, D. W., Pekar, S. F. & Pincay, V. Evidence for a heavily glaciated Antarctica during the late Oligocene "warming" (27.8–24.5 Ma): stable isotope records from ODP Site 690. *Paleoceanography* **32**, 384–396 (2017).
17. Jakob, K. A. et al. A new sea-level record for the Neogene/Quaternary boundary reveals transition to a more stable East Antarctic Ice Sheet. *Proc. Natl. Acad. Sci. USA* **117**, 30980–30987 (2020).
18. Norris, R. D. et al. Paleogene Newfoundland sediment drifts and MDHDS test. *Proc. Integr. Ocean. Drill. Progr.* **342**, 149 (2014).
19. van Peer, T. *Palaeomagnetic, Astrochronological, and Environmental Magnetic Perspective on Oligocene-miocene Climate, Using Drift Sediments from the Northwest Atlantic Ocean* (University of Southampton, 2017).
20. Levy, R. H. et al. Antarctic ice-sheet sensitivity to obliquity forcing enhanced through ocean connections. *Nat. Geosci.* **12**, 132–137 (2019).
21. Laskar, J. et al. A long-term numerical solution for the insolation quantities of the Earth. *Astron. Astrophys.* **428**, 261–285 (2004).
22. Raymo, M. E. & Nisancioglu, K. The 41 kyr world: Milankovitch's other unsolved mystery. *Paleoceanography* **18**, 1–6 (2003).
23. Lear, C. H., Rosenthal, Y., Coxall, H. K. & Wilson, P. A. Late Eocene to early Miocene ice sheet dynamics and the global carbon cycle. *Paleoceanography* **19**, 1–11 (2004).
24. Gasson, E., DeConto, R. M., Pollard, D. & Levy, R. H. Dynamic Antarctic ice sheet during the early to mid-Miocene. *Proc. Natl. Acad. Sci. USA* **113**, 3459–3464 (2016).
25. DeConto, R. M. et al. Thresholds for Cenozoic bipolar glaciation. *Nature* **455**, 652–656 (2008).
26. Fretwell, P. et al. Bedmap2: improved ice bed, surface and thickness datasets for Antarctica. *Cryosphere* **7**, 375–393 (2013).
27. Bohaty, S. M., Zachos, J. C. & Delaney, M. L. Foraminiferal Mg/Ca evidence for southern ocean cooling across the eocene-oligocene transition. *Earth Planet. Sci. Lett.* **317–318**, 251–261 (2012).
28. Eldrett, J. S., Harding, I. C., Wilson, P. A., Butler, E. & Roberts, A. P. Continental ice in Greenland during the Eocene and Oligocene. *Nature* **446**, 176–179 (2007).
29. St. John, K. Cenozoic ice-rafting history of the central Arctic Ocean: Terrigenous sands on the Lomonosov Ridge. *Paleoceanography* **23**, PA1S05 (2008).
30. Tripati, A. K. et al. Evidence for glaciation in the Northern Hemisphere back to 44 Ma from ice-rafted debris in the Greenland Sea. *Earth Planet. Sci. Lett.* **265**, 112–122 (2008).
31. Edgar, K. M., Pälike, H. & Wilson, P. A. Testing the impact of diagenesis on the δ18O and δ13C of benthic foraminiferal calcite from a sediment burial depth transect in the equatorial Pacific. *Paleoceanography* **28**, 468–480 (2013).
32. Moran, K. et al. The Cenozoic palaeoenvironment of the arctic ocean. *Nature* **441**, 601–605 (2006).
33. Wilson, D. S. et al. Antarctic topography at the Eocene-Oligocene boundary. *Palaeogeogr. Palaeoclimatol. Palaeoecol.* **335–336**, 24–34 (2012).
34. Paxman, G. J. G. et al. Reconstructions of Antarctic topography since the Eocene–Oligocene boundary. *Palaeogeogr. Palaeoclimatol. Palaeoecol.* **535**, 109346 (2019).
35. Paxman, G. J. G., Gasson, E. G. W., Jamieson, S. S. R., Bentley, M. J. & Ferraccioli, F. Long-term increase in Antarctic Ice Sheet vulnerability driven by bed topography evolution. *Geophys. Res. Lett.* **47**, e2020GL090003 (2020).
36. Hartman, J. D. et al. Paleoceanography and ice sheet variability offshore Wilkes Land, Antarctica-Part 3: insights from Oligocene-Miocene TEX86-based sea surface temperature reconstructions. *Clim. Past* **14**, 1275–1297 (2018).
37. Bijl, P. K. et al. Paleoceanography and ice sheet variability offshore Wilkes Land, Antarctica—Part 2: insights from Oligocene-Miocene dinoflagellate cyst assemblages. *Clim. Past* **14**, 1015–1033 (2018).
38. Troedson, A. L. & Smellie, J. L. The Polonez cove formation of King George Island, Antarctica: stratigraphy, facies and implications for mid-Cenozoic cryosphere development. *Sedimentology* **49**, 277–301 (2002).
39. Barrett, P. J. Cenozoic climate and sea level history from glacimarine strata off the Victoria Land Coast, Cape Roberts Project, Antarctica. in *Glacial Sedimentary Processes and Products* 259–287 (Blackwell Publishing Ltd., 2009). https://doi.org/10.1002/9781444304435.ch15.
40. De Vleeschouwer, D., Vahlenkamp, M., Crucifix, M. & Pälike, H. Alternating Southern and Northern Hemisphere climate response to astronomical forcing during the past 35 m.y. *Geology* **45**, 375–378 (2017).
41. Naish, T. R. et al. Obliquity-paced Pliocene West Antarctic ice sheet oscillations. *Nature* **458**, 322–328 (2009).
42. Duncan, B. et al. Climatic and tectonic drivers of late Oligocene Antarctic ice volume. *Nat. Geosci.* **15**, 819–825 (2022).
43. Spence, P. et al. Rapid subsurface warming and circulation changes of Antarctic coastal waters by poleward shifting winds. *Geophys. Res. Lett.* **41**, 4601–4610 (2014).
44. Toggweiler, J. R. & Russell, J. Ocean circulation in a warming climate. *Nature* **451**, 286–288 (2008).
45. Sosdian, S. M. & Rosenthal, Y. Deep-sea temperature and ice volume changes across the pliocene-pleistocene climate transitions. *Science.* **325**, 306–310 (2009).
46. Miller, K. G. et al. Cenozoic sea-level and cryospheric evolution from deep-sea geochemical and continental margin records. *Sci. Adv.* **6**, eaaz1346 (2020).
47. Rohling, E. J., Haigh, I. D., Foster, G. L., Roberts, A. P. & Grant, K. M. A geological perspective on potential future sea-level rise. *Sci. Rep.* **3**, 3461 (2013).
48. Zhang, Y. G., Pagani, M., Liu, Z., Bohaty, S. M. & Deconto, R. A 40-million-year history of atmospheric CO2. *Philos. Trans. R. Soc. A Math. Phys. Eng. Sci.* **371**, 20130096 (2013).
49. Martínez-Botí, M. A. et al. Plio-Pleistocene climate sensitivity evaluated using high-resolution CO2 records. *Nature* **518**, 49–54 (2015).
50. Sexton, P. F., Wilson, P. A. & Pearson, P. N. Microstructural and geochemical perspectives on planktic foraminiferal preservation: 'glassy' versus 'frosty'. *Geochem. Geophys. Geosystems* **7**, Q12P19 (2006).
51. Petrizzo, M. R., Leoni, G., Speijer, R. P., De Bernardi, B. & Felletti, F. Dissolution susceptibility of some paleogene planktonic foraminifera from ODP site 1209 (Shatsky Rise, Pacific Ocean). *J. Foraminifer. Res.* **38**, 357–371 (2008).
52. Andersson, C. Pliocene calcium carbonate sedimentation patterns of the Ontong Java Plateau: ODP sites 804 and 806. *Mar. Geol.* **150**, 51–71 (1998).
53. Coxall, H. K. & Wilson, P. A. Early oligocene glaciation and productivity in the eastern equatorial pacific: insights into global carbon cycling. *Paleoceanography* **26**, PA2221 (2011).

54. Coxall, H. K. et al. Export of nutrient rich northern component water preceded early oligocene Antarctic glaciation /704/106/413 /704/829 /704/106/2738 article. *Nat. Geosci.* **11**, 190–196 (2018).
55. Katz, M. E. et al. Early Cenozoic benthic foraminiferal isotopes: species reliability and interspecies correction factors. *Paleoceanography* **18**, 1024 (2003).
56. Barker, S., Greaves, M. & Elderfield, H. A study of cleaning procedures used for foraminiferal Mg/Ca paleothermometry. *Geochem. Geophys. Geosystems* **4**, 1–20 (2003).
57. Bian, N. & Martin, P. A. Investigating the fidelity of Mg/Ca and other elemental data from reductively cleaned planktonic foraminifera. *Paleoceanography* **25**, PA2215 (2010).
58. Greaves, M. et al. Interlaboratory comparison study of calibration standards for foraminiferal Mg/Ca thermometry. *Geochem. Geophys. Geosystems* **9**, Q08010 (2008).
59. Lear, C. H., Rosenthal, Y. & Slowey, N. Benthic foraminiferal Mg/Ca-paleothermometry: a revised core-top calibration. *Geochim. Cosmochim. Acta* **66**, 3375–3387 (2002).
60. Barrientos, N. et al. Arctic Ocean benthic foraminifera Mg/Ca ratios and global Mg/Ca-temperature calibrations: new constraints at low temperatures. *Geochim. Cosmochim. Acta* **236**, 240–259 (2018).
61. Rausch, S., Böhm, F., Bach, W., Klügel, A. & Eisenhauer, A. Calcium carbonate veins in ocean crust record a threefold increase of seawater Mg/Ca in the past 30 million years. *Earth Planet. Sci. Lett.* **362**, 215–224 (2013).
62. Dickson, J. A. D. Fossil echinoderms as monitor of the Mg/Ca ratio of Phanerozoic oceans. *Science.* **298**, 1222–1224 (2002).
63. Lear, C. H. et al. Neogene ice volume and ocean temperatures: insights from infaunal foraminiferal Mg/Ca paleothermometry. *Paleoceanography* **30**, 1437–1454 (2015).
64. Shackleton, N. J. Attainment of isotopic equilibrium between ocean water and the benthonic foraminifera genus Uvigerina: isotopic changes in the ocean during the last glacial. *Cent. Natl. Rech. Sci. Colloq. Int.* **219**, 203–210 (1974).
65. Harreither, W., Nicholls, P., Sygmund, C., Gorton, L. & Ludwig, R. Investigation of the pH-dependent electron transfer mechanism of ascomycetous class II cellobiose dehydrogenases on electrodes. *Langmuir* **28**, 6714–6723 (2012).
66. Schulz, M. & Mudelsee, M. REDFIT: estimating red-noise spectra directly from unevenly spaced paleoclimatic time series. *Comput. Geosci.* **28**, 421–426 (2002).
67. Hammer, Ø., Harper, D. A. T. & Ryan, P. D. Past: paleontological statistics software package for education and data analysis. *Palaeontol. Electron.* **4**, 9 (2001).
68. Paillard, D., Labeyrie, L. & Yiou, P. Macintosh program performs time-series analysis. *Eos. Trans. Am. Geophys. Union* **77**, 379–379 (1996).

Acknowledgements

We thank B. Hennrich, F. Kerschhofer, and P. Geppert for laboratory assistance, A. Bahr for his support in statistical analyses, C. Scholz and S. Rheinberger for support during ICP-OES measurements, and B. Knape, M. Greule and F. Keppler for support during stable isotope measurements. We thank the Captain, crew, JRSO technical staff, and shipboard scientists onboard the R/V JOIDES Resolution during IODP Expedition 342. This research used samples provided by the Integrated Ocean Drilling Programme (IODP). Funding for this study was provided by the German Research Foundation (grants FR2544/12 and FR2544/17 to S.B. and O.F.; BO2505/9 to A.B.), the Natural Environment Research Council (NERC) (grants NE/R018235/1 and NE/T012285/1 to T.E.v.P.; NE/K014137/1 to D.L.). P.A.W. acknowledges funding from NERC (grant NE/D006465/1) and the Royal Society (Wolfson Merit Award).

Author contributions

S.B., A.B. and O.F. conceived the study, generated data. S.B. lead data analysis with input from A.B., D.L., T.E.v.P., P.A.W. and O.F. S.B., P.A.W. and O.F. wrote the manuscript. All authors provided critical feedback and helped shape the research, analysis, and manuscript.

Funding

Open Access funding enabled and organized by Projekt DEAL.

Competing interests

The authors declare no competing interests.

Additional information

Supplementary information The online version contains supplementary material available at https://doi.org/10.1038/s43247-023-00864-9.

Correspondence and requests for materials should be addressed to Swaantje Brzelinski.

Peer review information *Communications Earth & Environment* thanks the other, anonymous, reviewer(s) for their contribution to the peer review of this work. Primary Handling Editor: Joe Aslin.

Reprints and permission information is available at http://www.nature.com/reprints

Publisher's note Springer Nature remains neutral with regard to jurisdictional claims in published maps and institutional affiliations.